Petroleum Science 21 (2024) 1915–1927

Contents lists available at ScienceDirect

Petroleum Science

journal homepage: www.keaipublishing.com/en/journals/petroleum-science

Original Paper

Experimental study of the influencing factors and mechanisms of the pressure-reduction and augmented injection effect by nanoparticles in ultra-low permeability reservoirs

Pan Wang [a, b], Yu-Hang Hu [a, b], Liao-Yuan Zhang [c], Yong Meng [c], Zhen-Fu Ma [d], Tian-Ru Wang [a, b], Zi-Lin Zhang [c], Ji-Chao Fang [f], Xiao-Qiang Liu [a, b], Qing You [a, b, *], Yan Zhang [b, e, **]

[a] Beijing Key Laboratory of Unconventional Natural Gas Geological Evaluation and Development Engineering, China University of Geosciences (Beijing), Beijing, 100083, China
[b] School of Energy Resources, China University of Geosciences (Beijing), Beijing, 100083, China
[c] Petroleum Engineering Technology Research Institute, Sinopec Shengli Oilfield Company, Dongying, 257000, Shandong, China
[d] Hekou Oil Production Plant, Sinopec Shengli Oilfield Company, Dongying, 257200, Shandong, China
[e] CNPC Engineering Technology R&D Company Limited, Beijing, 102206, China
[f] Petroleum Exploration and Production Research Institute, SINOPEC, Beijing, 102206, China

ARTICLE INFO

Article history:
Received 14 March 2023
Received in revised form
23 November 2023
Accepted 24 November 2023
Available online 29 November 2023

Edited by Yan-Hua Sun and Meng-Jiao Zhou

Keywords:
Nanoparticle
Pressure reduction
Augmented injection
Ultra-low permeability reservoir

ABSTRACT

Nanoparticles (NPs) have gained significant attention as a functional material due to their ability to effectively enhance pressure reduction in injection processes in ultra-low permeability reservoirs. NPs are typically studied in controlled laboratory conditions, and their behavior in real-world, complex environments such as ultra-low permeability reservoirs, is not well understood due to the limited scope of their applications. This study investigates the efficacy and underlying mechanisms of NPs in decreasing injection pressure under various injection conditions (25–85 °C, 10–25 MPa). The results reveal that under optimal injection conditions, NPs effectively reduce injection pressure by a maximum of 22.77% in core experiment. The pressure reduction rate is found to be positively correlated with oil saturation and permeability, and negatively correlated with temperature and salinity. Furthermore, particle image velocimetry (PIV) experiments (25 °C, atmospheric pressure) indicate that the pressure reduction is achieved by NPs through the reduction of wall shear resistance and wettability change. This work has important implications for the design of water injection strategies in ultra-low permeability reservoirs.

1. Introduction

Low-porosity and low-permeability sandstone reservoirs, which were previously difficult to exploit, have become a vital part of the global oil industry (Asif and Muneer, 2007; Zheng et al., 2017; Hu et al., 2018), also facing some challenges including poor fluid permeability, low productivity, small pore throat radius, and high sensitivity to external phases for them. Water injection development in such reservoirs can lead to serious water-sensitive and water-lock damages, resulting in high injection pressure in the injection well and other issues (Zhai et al., 2018). NPs have been the subject of numerous studies for oil field development, and field tests have shown that they can effectively reduce water injection pressure, increase injection volume, and augment the energy of low-permeability formations in low-permeability reservoirs (Yekeen et al., 2019; Roustaei et al., 2013).

NPs are solids or thin films with particle or grain sizes in the nanometer range (Turan et al., 2019). Due to their extremely small size, large specific surface area, and high atomic ratio at grain boundaries, NPs exhibit unique properties in various fields such as chemistry, optics, thermodynamics, electronics, mechanics, and

* Corresponding author. Beijing Key Laboratory of Unconventional Natural Gas Geological Evaluation and Development Engineering, China University of Geosciences (Beijing), Beijing, 100083, China.
** Corresponding author. School of Energy Resources, China University of Geosciences (Beijing), Beijing, 100083, China.
E-mail addresses: youqing@cugb.edu.cn (Q. You), zgsydxzy@163.com (Y. Zhang).

https://doi.org/10.1016/j.petsci.2023.11.024

acoustics, stemming from surface, quantum size, and macroscopic quantum tunneling effects. NPs have a wide range of applications, including in the chemical industry, biological industry, manufacturing of mechanical materials, and precision electronic devices (Kaibo et al., 2020). Among the various types of NPs, silica (SiO_2) nanoparticles are white amorphous flocculent powder that is non-toxic, odorless, and environmentally friendly. It has become one of the most widely industrialized NPs at the global level (Idris et al., 2020; Wasan and Nikolov, 2003).

In the 1960s, several countries began to investigate the utilization of NPs in the oil and gas industry and achieved significant progress. For instance, in 1966, the Soviet Union successfully applied silica NPs in water injection wells at the Romaskin Oilfield, which resulted in a reduction of the injection pressure and an increase in injection volume (Ding, 2004; Ke and Wei, 2008). Subsequently, silica NPs were applied to 39 water injection wells in the Bayukhov Oilfield. The treatment led to an increase in injection volume by 1.1–8.0 times and significantly improved the crude oil recovery rate. The positive effects are believed to be due to the ability of the thin nano-film to substitute the thicker hydration layer adsorbed on the pore wall, which effectively enlarges the sizes of flow channels (Dai et al., 2015). Cottin et al. (2003) studied the laws governing fluid movement in microchannels within rocks, and established that by increasing the wettability and roughness of the pore surface, the fraction of fluid as it passes through the rock can be greatly reduced. Building on this research, it was subsequently determined that the reduction in pressure was primarily a result of the slip phenomenon of the water phase on the hydrophobic NP adsorption (Di et al., 2007; Lauga et al., 2007). Suleimanov et al. (2011) demonstrated that the addition of NPs to the oil displacement agent increases the recovery from heterogeneous and homogeneous porous media by 35% and 17%, respectively, at 25 °C, as compared to the use of surfactants alone. The authors also found that wettability of rock surface remained largely unchanged after the addition of NPs, the recovery improvement was observed due to the reduction of interfacial tension caused by NPs and shift in fluid flow behavior in the pores, from Newtonian to non-Newtonian. The commonly accepted mechanisms that explain the enhanced oil recovery effect of NPs are i) the reduction of the interfacial tension between two phases, and ii) the alteration of the wettability of the rock surface (Zhang et al., 2014; Hendraningrat and Torsæter, 2014; Ali et al., 2018).

Following the study of polysilicon NPs in the 1990s, research on the pressure-reducing properties of NPs experienced significant growth in China (Qu, 2008). Lu et al. (2003) proposed that the principal mechanisms contributing to the pressure-reduction performance of NPs include: i) the substitution of the water film adsorbed on the pore wall surface leading to the expansion of the effective pore diameter, and ii) the reduction of resistance within the pores resulting from the hydrophobicity-induced prohibition of the hydration expansion of clay minerals. Wang et al. (2003) established that the optimal injection volume and the optimal concentration of NPs were 0.6 PV (pore volume) and 0.5 wt%, respectively, which resulted in a 52.78% decrease in injection pressure and a 6.84% increase in oil recovery. Sun et al. (2006) conducted experimental studies of the impact of polysilicon material products on rock wettability, the correlation between treatment efficacy and core permeability, and the effect of permeability on the treatment efficacy of core wettability. Both laboratory and field tests confirm that the injection of polysilicon NPs has a positive effect on reducing core injection pressure, increasing core seepage capacity, and shifting the wettability of cores from water-wet to oil-wet after prolonged water injection, thus improving water injection channels and augmenting water injection capacity.

In summary, the utilization of NPs for pressure reduction represents an effective solution during water injection development in ultra-low permeability reservoirs. Additionally, the implementation of NPs is relatively straightforward and causes minimal pollution. Despite their frequent and effective utilization in ultra-low permeability reservoirs, our understanding of the underlying mechanisms behind the pressure-reducing properties of NPs is still limited, and further research is needed to understand the influence of various factors on their practical application. In this study, we utilized NPs with a small particle size, low dispersion viscosity, and high stability that have been previously demonstrated to have the ability to reduce pressure and increase injection volume (Wang et al., 2018; Hu et al., 2020). These NPs were then subjected to physical experiments to investigate the factors that influence their performance. Variations in pressure-reducing and injection-increasing performance of NPs were investigated under different dispersion concentrations, adsorption time, injection volume, core permeability, reservoir temperature, and oil saturation. The underlying mechanisms of these factors were subsequently established. Our findings offer guidance and a theoretical basis for the utilization of NPs in the development of ultra-low permeability reservoir, allowing for the optimization of the injection and production process to maximize the pressure reduction and injection increasing performance. Additionally, the research explained the mechanism of NPs reducing the flow resistance of water in channels macroscopically and microscopically, which can provide some reference for the follow-up research on pressure reduction of NPs.

2. Materials and methods

2.1. Experimental materials

Sandstone core sample used were obtained from outcrops procured from the Beijing Huanyu Petroleum Technical Service Company, China. The mineral composition of these core samples was analyzed using X-ray diffraction (XRD) which revealed that they primarily composed of quartz, potassium feldspar, plagioclase, and clay minerals, with the content of quartz being greater than 85%. Furthermore, the gas permeability of these core samples was found to range from 0.1 to 1.0 mD (Table 1).

Pore throat size distribution of core samples was also analyzed.

Table 1
Properties of the core samples used.

Core No.	Diameter, cm	Length, cm	Porosity, %	Permeability, mD
1-1	2.51	4.95	15.3	0.905
1-2	2.50	4.92	16.1	0.803
1-3	2.52	5.01	15.4	0.892
1-4	2.48	4.97	13.6	0.821
2-1	2.59	5.00	13.7	0.878
2-2	2.44	4.91	15.0	0.888
2-3	2.49	5.02	14.1	0.899
3-1	2.49	4.99	13.7	0.721
3-2	2.52	4.97	14.9	0.878
3-3	2.46	5.03	15.7	0.894
4-1	2.48	4.94	14.2	0.659
4-2	2.52	5.02	14.1	0.693
4-3	2.53	5.09	12.9	0.674
5-1	2.45	4.93	10.9	0.093
5-2	2.55	5.09	13.3	0.318
5-3	2.50	5.06	17.7	0.980
6-1	2.48	5.02	15.8	0.948
6-2	2.46	5.07	16.1	1.034
6-3	2.51	4.98	16.4	1.028
7-1	2.45	5.03	14.5	0.984
7-2	2.53	4.96	14.4	1.061
7-3	2.52	5.07	15.7	0.996

The distribution of pore throat radius of two core samples (No. 4-1 and No. 5-2) was determined through mercury injection testing, and the resulting pore throat distribution is depicted in Fig. 1. Calculations reveal that the mean pore throat diameter remains within the range from approximately 0.5 to 1 μm.

In this study, NPs were synthesized in laboratory following the methods previously described by our group (Hu et al., 2020). The NPs are pH-sensitive and functional, with a stabilized particle size of around 15 nm when the pH is greater than or equal to 10 (as indicated in Fig. 2(a)). The morphological characteristics of the NPs are depicted in Fig. 2(b).

In this study, a synthetic oil composed of a blend of crude oil and kerosene was utilized, which exhibits a viscosity of 2.40 mPa s (50 °C) and a density of 0.820 g/cm^3 at 25 °C.

Table 2 lists the properties of synthetic brine that simulates the composition of formation water in the Shengli Oilfield.

2.2. Experimental method

In this research core experiments were initially conducted and the adsorption rate of NPs was measured to analyze the impact of several influencing factors on the efficacy of pressure reduction and augmented injection during oilfield water injection process. Subsequently, to investigate the microscopic mechanism of pressure reduction attributed to NPs, particle image velocimetry (PIV) and wettability experiments were undertaken to assess the influence of NPs on the fluid flow dynamics within microchannels.

2.2.1. Pressure-reduction capacity

Experiments to investigate the pressure reduction rate of NPs were conducted using a laboratory setup shown in Fig. 3. The injection volume and pressure were regulated by an ISCO pump. The sandstone core samples, considering the oil saturation in the effective pores can be regarded as zero in the near wellbore zone of water injection wells in oil fields, were first saturated only with synthetic brine and then placed in a core holder and subjected to a confining pressure of 15 MPa. Water flooding was performed at a constant injection rate of 0.5 mL/min, and the injection pressure was recorded until the pressure reaches stability.

Then, the NP suspension was injected into the core sample at a predetermined concentration and volume, after which both ends of the core holder were sealed to enable NP adsorption. The water flooding was then resumed at the initial injection rate. The stable pressure at the injection port was compared before and after NP treatment to calculate the pressure reduction rate, which was determined using the following equation:

$$E_{pd} = \frac{P_b - P_a}{P_b} \quad (1)$$

where E_{pd} represents the pressure drop rate, expressed as a percentage; P_b is the stable water flooding pressure before NP treatment, MPa; P_a is the stable water flooding pressure after NP treatment, MPa.

The objective of changing various influencing factors, such as the concentration, adsorption time, displacement rate, temperature, and salinity of the injected nanoparticle dispersion solution, was to examine the impact of these different factors on the rate of pressure reduction.

2.2.2. Micro-flow visualization of NPs

In order to visualize the flow of NPs, we applied a magnification factor of 300 to the relevant parameters associated with the core dimensions, resulting in an amplification of the flow rate from its initial average of 0.02–6 cm/s, and an augmentation of the channel size from the initial average of 1–300 μm. Therefore, a scaled-up microfluidic device was utilized in this study. The device was made by milling a 200 mm × 80 mm × 10 mm plate of polymethyl methacrylate (PMMA) and sealing it with another 200 mm × 80 mm × 5 mm PMMA plate, as shown in Fig. 4 and Table 3. The pore–throat ratio of the microfluidic chip was 3:1.

The flow of NPs was visualized using micro-particle image velocimetry (μPIV), a system capable of capturing the image of fluorescent tracer particles via a high-speed camera. The images were processed through a sophisticated PIV algorithm, allowing the researchers to obtain the flow field within the microchannel. By analyzing the flow dynamics of nanofluids in a microchannel, the effects of NPs on fluid flow resistance could be studied. During the microfluidic experiment, when the pressure difference was set to 1.5 kPa, the measurement section was located approximately 7.0–7.3 mm from the inlet. However, when the pressure difference was increased to 2.5 kPa, the measurement section shifted backwards and was situated approximately 50.0–50.3 mm from the inlet, the measurement section is far from the throat, so it can be sure to keep the flow condition steady during the measurement.

The fluid was introduced into the microfluidic device by gravity flow (Fig. 5), as the pore volume of the chip is negligible compared

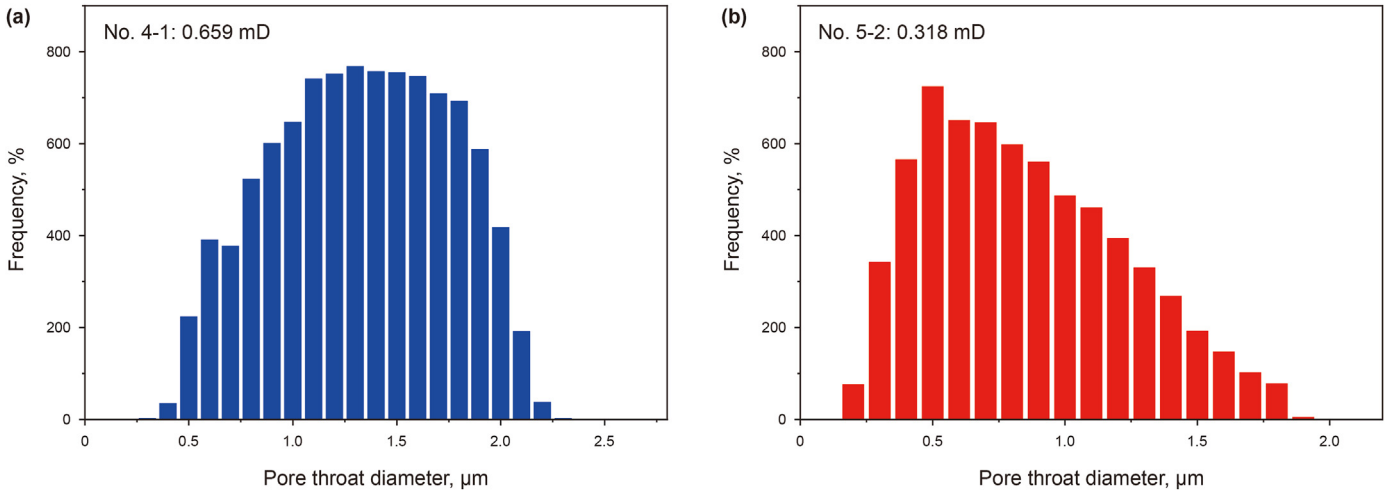

Fig. 1. Pore throat size distribution of No. 4-1 (**a**) and No. 5-2 (**b**).

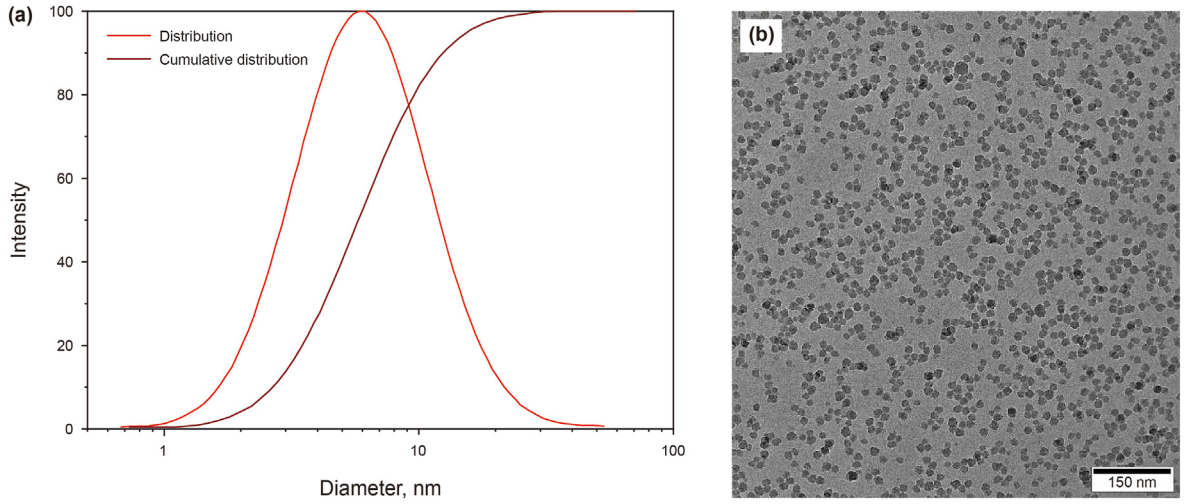

Fig. 2. NP characteristics. (**a**) Particle size distribution; (**b**) Morphological characteristics.

Table 2
Properties of synthetic brine.

pH	Cation concentration, mg/L				Total salinity, mg/L
	Na^+	K^+	Ca^{2+}	Mg^{2+}	
8.0	16460	315	408	371	17554

to the fluid container (diameter of 52 mm) and the injection rate is small (<100 mm/s). As a result, the injection can be considered as a constant pressure injection process in the system. The pressure difference between the outlet and inlet of the chip, known as the injection pressure (P_{in}), can be calculated as

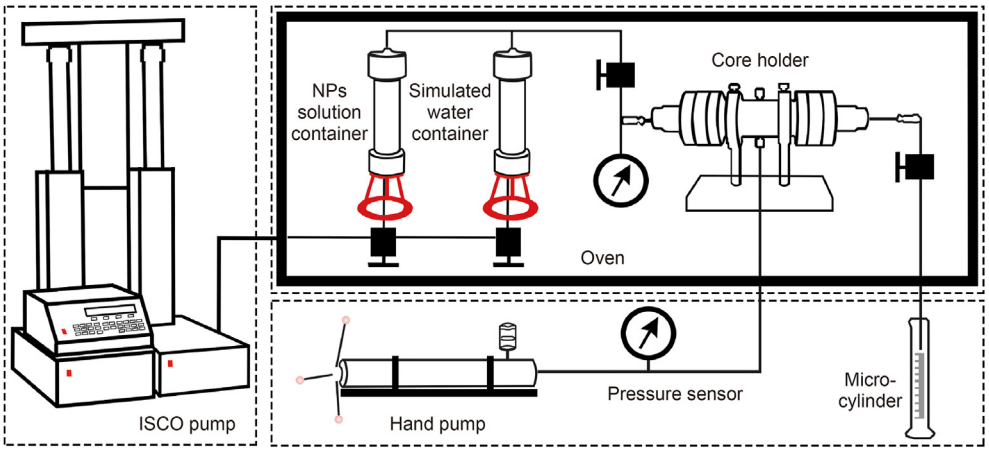

Fig. 3. Schematic of core flooding experimental setup.

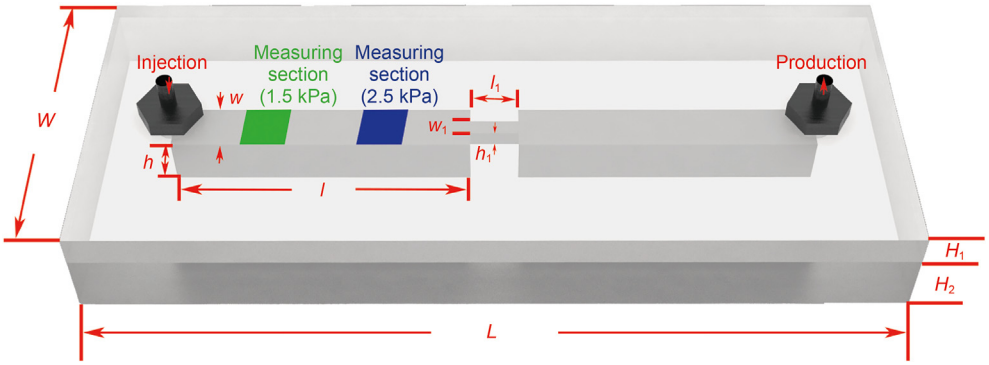

Fig. 4. Schematic of microfluidic device.

Table 3
Dimension of microfluidic device.

L, mm	W, mm	H_1, mm	H_2, mm	l, mm	w, mm	h, mm	l_1, mm	w_1, mm	h_1, mm
200	80	10	5	80	0.3	0.3	0.2	0.1	0.1

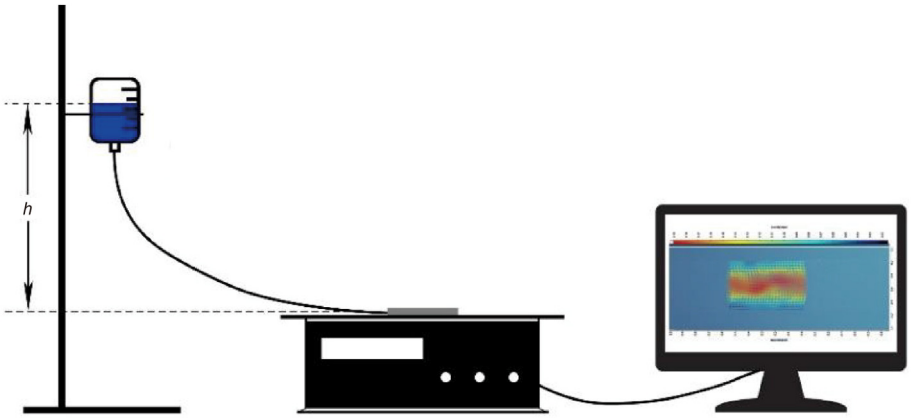

Fig. 5. Schematic of experimental device.

$$P_{\text{in}} = \rho \cdot g \cdot h \tag{2}$$

where ρ is the density of the fluid; g is the acceleration due to gravity; and h is the height difference between the top of the fluid level and the surface of the microfluidic device.

2.2.3. Wettability analysis

The experiments were carried out to study the wettability of core slices and microfluidic chips. Initial measurements entailed the determination of water contact angles exhibited by polished core slice and microfluidic chips. Following marking the measurement position, both samples were subjected to immersion within a 0.05 wt% NP dispersion for a duration of 36 h. Subsequent to immersion, a slowly rinse with deionized water was administered to the test surfaces, succeeded by a desiccation process within a 50 °C oven. Ultimately, the water contact angles of the desiccated core slice and microfluidic chips were measured, consistently at the previously marked positions.

2.2.4. Adsorption rate analysis

Ultraviolet spectrophotometry analyses were conducted to quantify the adsorption quantities of NPs within the porous media. The experimental process was initiated by establishing a standardized curve that correlates alterations in concentration with absorbance. Following this, NP dispersion was injected (1 pore volume (PV)) into the rock core and allowed to stabilize over a 36-h period. Subsequently, a water flush was conducted until the produced fluid no longer contained any traces of NPs. Finally, the concentration of the produced fluid was measured by spectrophotometry to compute the adsorption rate ($R_{\text{adsorption}}$) in Eq. (3). The standardized curve depicting the relationship between concentration changes and absorbance, is presented in Fig. 6.

$$R_{\text{adsporption}} = \frac{m_{\text{injection}} - m_{\text{production}}}{m_{\text{core}}} \tag{3}$$

where $m_{\text{injection}}$ is the mass of NPs in injected fluid; $m_{\text{production}}$ is the mass of NPs in production fluid; m_{core} is the mass of core.

3. Results and discussion

We utilized an ultra-low permeability core and microfluidic device to simulate a tight oil reservoir and monitored changes in the injection pressure and flow field during the displacement process. The purpose of this was to investigate the pressure-reducing ability and mechanisms of the NPs.

3.1. Influencing factors of pressure-reduction and augmented injection abilities of NPs

The influence of seven factors on the pressure-reducing capability of NPs were investigated. These factors were concentration, adsorption time, injection volume, permeability, oil saturation, temperature, and salinity. The experiment was designed such that every factor was analyzed through 3 to 4 of the 27 sets of core experiments conducted, as shown in Table 4.

Fig. 7(a)–(c) shows that NPs can reduce the injection pressure (10%–25%) of ultra-low permeability cores. As shown in Fig. 7(d), the particle size of NPs keeps stability at approximately 15 nm at room temperature and zero salinity. This particle size remains smaller than the average pore throat diameter ranging from 0.5 to 1 μm. With increases in NP concentration, adsorption time and injection volume, the pressure reduction rates increase first and then decrease a little, the common point of these three factors is that they all effect the nanoparticle adsorption capacity on the rock. Fig. 8 reveals that with an increase in NP concentration, the adsorbed nanoparticles within the core exhibit gradual augmentation, a turning point emerges at a concentration of 0.05 wt%, aligning concordantly with the experimental pressure reduction rate results as shown in Fig. 7(a). Therefore, the mechanisms of experimental results in Fig. 7 can be explained that the pore surface is uneven at first, so there is a large resistance between the fluid boundary and the rock surface (Fig. 9(a)). With an increase in adsorption capacity, NPs preferentially may adsorb in concave positions, the rock surface can be flatter (Fig. 9(b) and (c)), so that flow resistance decreases. The results agree with the results reported by other researchers (Kong et al., 2022), The adsorption of NPs on the solid surface induces a mitigation of surface roughness, engenders a reduction in frictional resistance attributable to the rolling effect,

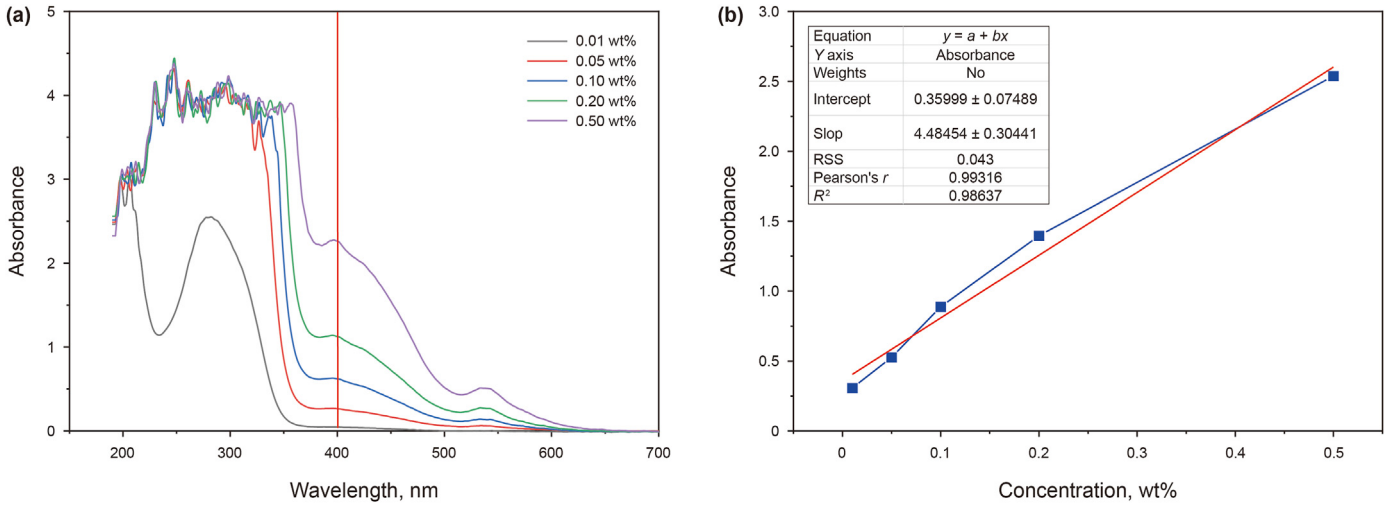

Fig. 6. Standardized curve correlates concentration alteration with absorbance.

Table 4
Factor values corresponding to the results of Figs. 7, 10 and 13 of all conducted core experiments.

	NP oncentration, wt%	Injection volume, PV	Adsorption, h	Permeability, mD	Oil saturation, %	Temperature, °C	Salinity, mg/L	Core used
Fig. 7(a)	/	1	36	—	0	25	0	No. 1-1 to No. 1-4
Fig. 7(b)	0.05	/	36	—	0	25	0	No. 1-1, No. 2-1 to No. 2-3
Fig. 7(c)	0.05	1	/	—	0	25	0	No. 1-1, No. 3-1 to No. 3-3
Fig. 10(a)	0.05	1	36	—	0	25	0	No. 4-1 to No. 4-3
Fig. 10(b)	0.05	1	36	—	/	25	0	No. 4-1, No. 5-1 to No. 5-3
Fig. 13(a)	0.05	1	36	—	0	/	0	No. 1-1, No. 6-1 to No. 6-3
Fig. 13(b)	0.05	1	36	—	0	25	/	No. 1-1, No. 7-1 to No. 7-3

Note: "/" indicates the value can be seen in each figure; "—" indicates the value can be looked up in Table 1 through core number.

consequently, so the impediment posed by fluid flow across the surface experiences a corresponding diminution. However, excess NPs form multilayer adsorption on the rock surface, the adsorption layer makes the pore flow space smaller, and the pressure reduction rate decreases (Fig. 9(d)).

Fig. 10 demonstrates a positive relationship between the pressure reduction rate and both oil saturation and permeability, which have an impact on the flow space available for the injected fluid. The higher the oil saturation in the core, the smaller the space available for water to flow. According to previous study (Nikolov et al., 2010), NPs have been found to be more effective at removing the oil layer from the rock surface compared to water. As a result, the "pore enlargement" effect produced by NPs is more pronounced in cores with a higher oil saturation (Fig. 11), and the result agrees to the research result of Wang et al. (2022). Conversely, as the permeability decreases and the pore size becomes smaller (Fig. 12), the adsorption of NPs may further decreases the effective pore size, resulting in a weakened pressure reduction effect of NPs in the cases of extremely low permeability.

The results depicted in Fig. 13 indicate the negative correlation between the pressure reduction rate and temperature, as well as pressure reduction rate and salinity, because temperature and salinity can affect the stability of NPs. To assess the stability of NPs across varying temperatures and salinity levels, we prepared NPs at a concentration of 0.05 wt% in different temperature ovens of 60–105 °C (0 salinity) and different salinity (from 10,000 to 50,000 mg/L) at 25 °C. After undergoing a 30-min stabilization, we applied dynamic light scattering (DLS) to measure the particle size and ζ potential under these diverse conditions, and the results are shown in Fig. 14. The results reveal that with increases in temperature and salinity, the ζ potential of NPs decreases and its dispersion stability decreases. Consequently, the NPs exhibit a propensity to aggregate into larger entities, resulting in potential core damage and a concomitant attenuation in pressure reduction capability.

3.2. Nanoparticle pressure-reduction mechanisms in microfluidic devices

The core experiments indicate that NPs have a significant impact on the macro injection pressure, and this effect is due to the adsorption of NPs on the porous media. To verify this further, additional microfluidic flooding experiments were carried out.

Microfluidic flooding experiments were conducted under pressure differences of 1.5 and 2.5 kPa. The flow resistance was calculated using Eq. (3), and the results of PIV using different nanoparticle concentrations (0, 0.01, and 0.05 wt%) were obtained and presented.

It has been observed that, compared to the flow of water alone (Fig. 15(a)), the flow rate in a microchannel can be increased when NPs are present. With the introduction of NPs (0.01 wt%, Fig. 15(b)), the average flow rate increases by 39.4%. Further increasing the concentration of NPs to 0.05 wt% results in an additional increase in the average flow rate by 49.5% (Fig. 15(c)). The increase in flow velocity, resulting from the same pressure drop, results in a change in the cross-sectional flow field from a U-shape to a trapezoidal shape. Additionally, the faster the velocity, the wider the trapezoidal plateau becomes.

At a pressure difference of 2.5 kPa, the flow rate in the microchannel is increased by 14.5%–28.1% as the concentration of NPs increases (Fig. 16(a)–(c)). As compared to the flow field cross-section at a pressure difference of 1.5 kPa, the shape of the flow

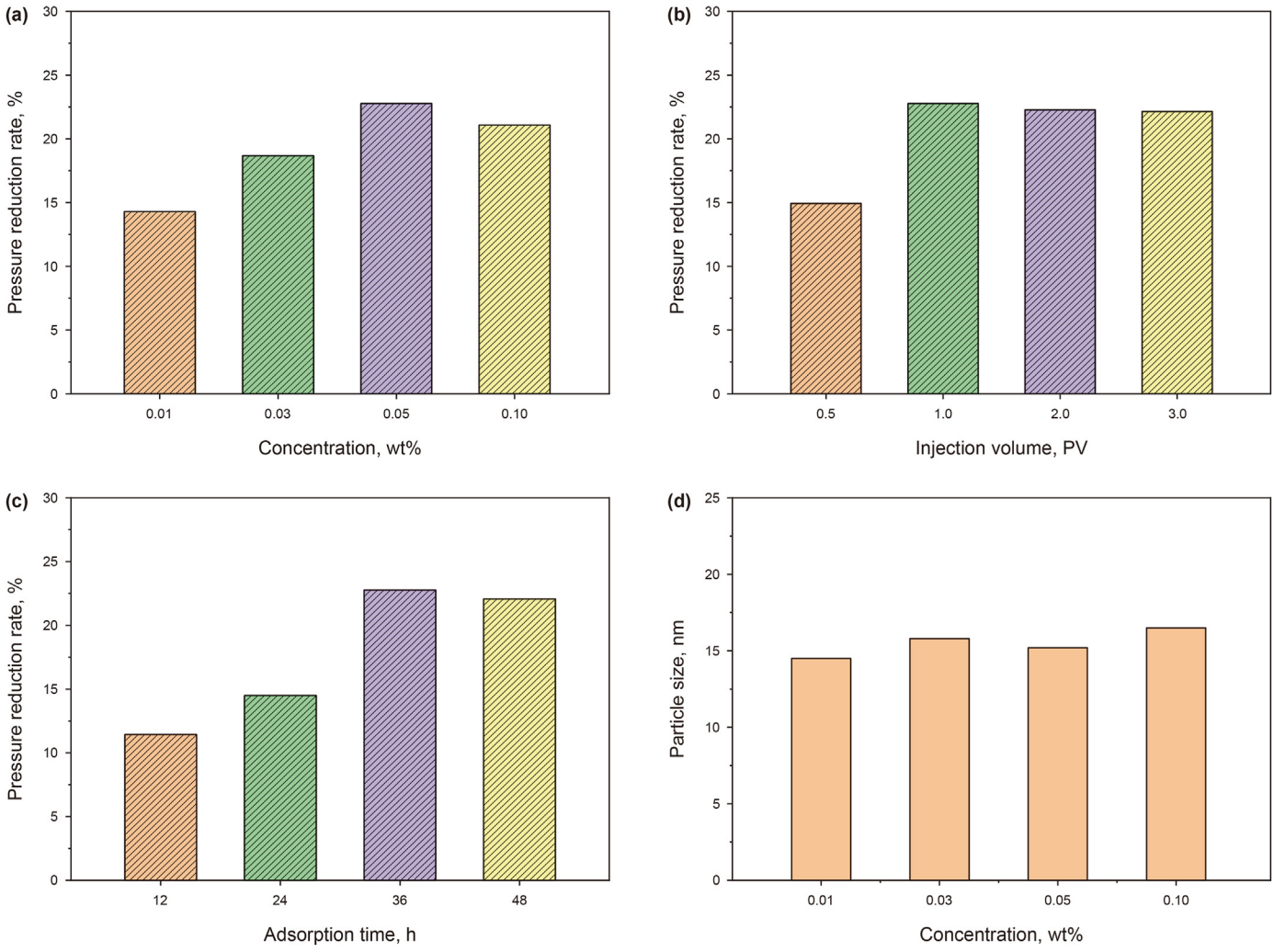

Fig. 7. Pressure reduction rate at different NP concentrations (**a**), injection volumes (**b**), and adsorption time (**c**). **(d)** Particle size at different concentrations.

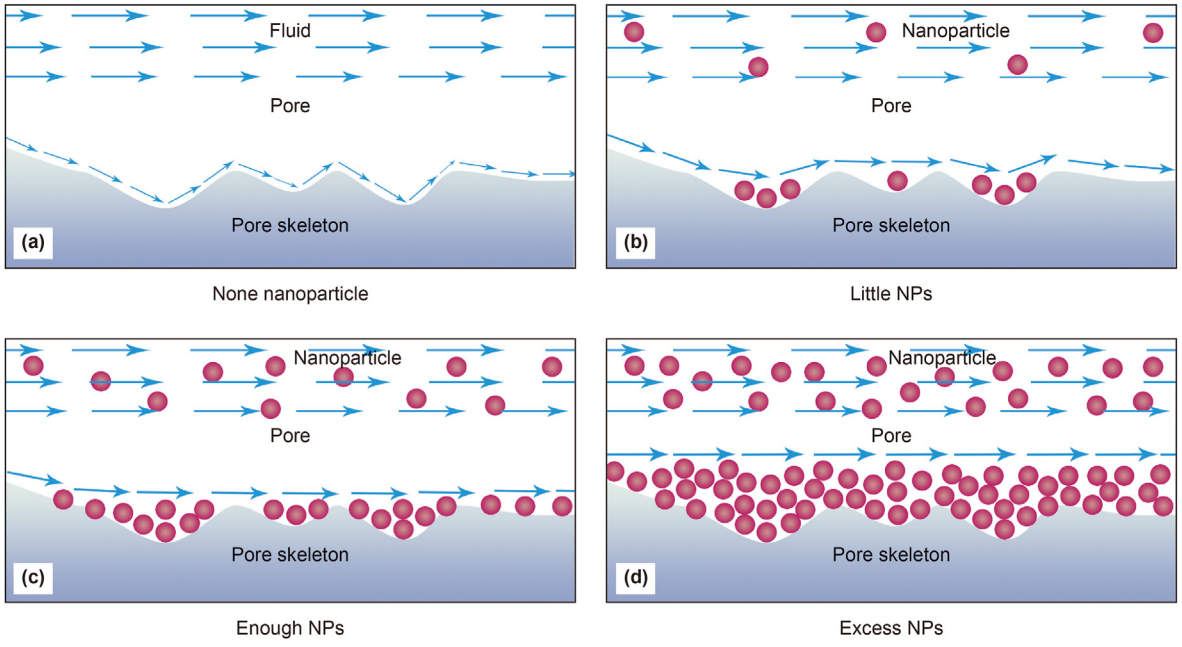

Fig. 8. Adsorption rate at different NP concentrations.

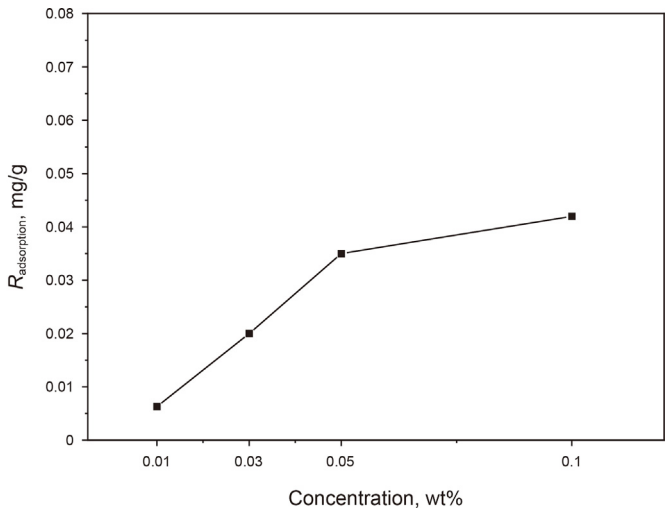

Fig. 9. Adsorption capacity of NPs on the rock surface.

field cross-section in the microchannel becomes spiker with increasing NP concentration. The ability of NPs to enhance the flow velocity was found to decrease with increasing pressure difference, even at the same concentration of NPs. For instance, at a concentration of 0.01 wt% of NPs, a 39.4% increase in the flow rate was achieved at a pressure difference of 1.5 kPa, whereas only a 14.5% increase was observed at a pressure difference of 2.5 kPa. A similar trend was observed for a concentration of 0.05 wt% of NPs, where a 49.5% increase in the flow rate was observed at a pressure difference of 1.5 kPa, but only a 28.1% increase was observed at a pressure difference of 2.5 kPa. These results suggest that the effects of pressure reduction and augmented injection decreases with the increase in flow rate. This provides further insight into the relationship between the pressure reduction rate and permeability shown in Fig. 10, where fluid flow is slower at high permeability cores, leading to a higher pressure-reduction rate, given the same flow flux.

The results of PIV experiments reveal the difference in the shape of the flow field before and after NP adsorption onto the flow channel wall, influenced by diverse injection pressure. According to

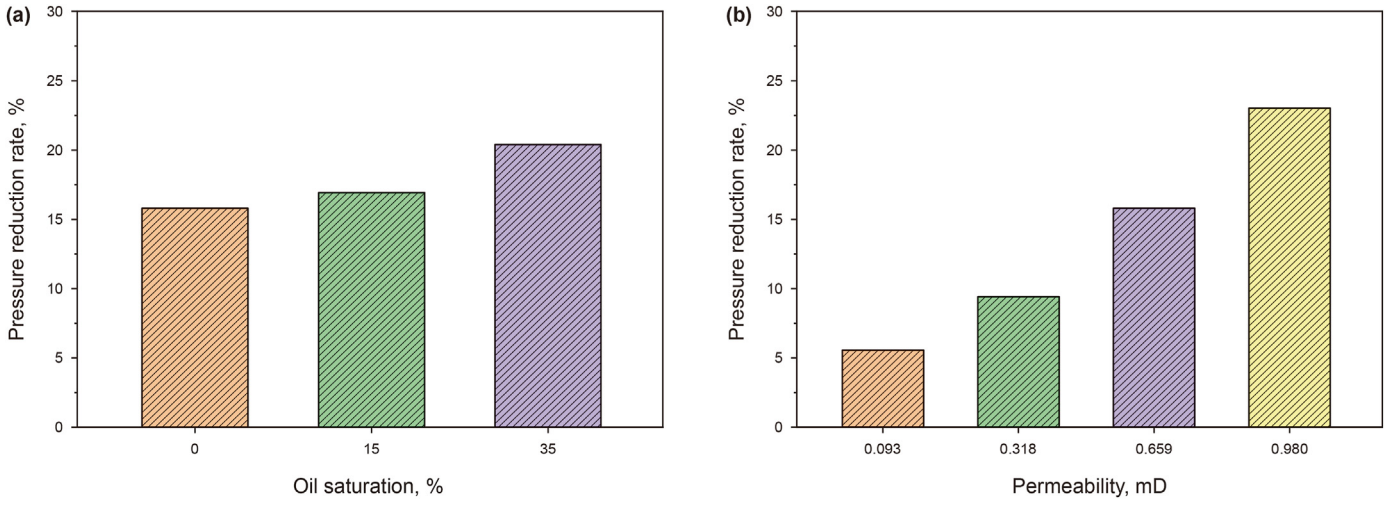

Fig. 10. Pressure reduction rate at different oil saturation (**a**) and permeability (**b**).

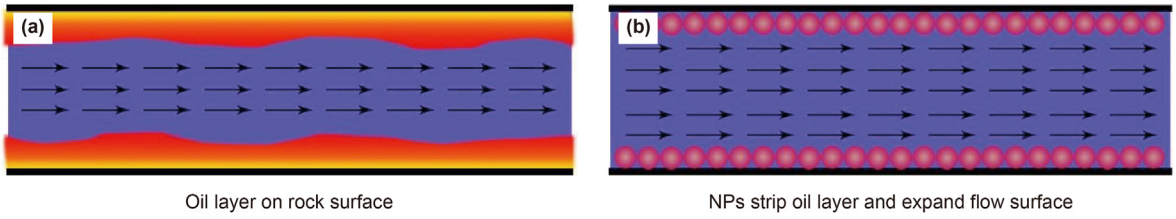

Fig. 11. The oil layer on rock surface affects the size of the flow space.

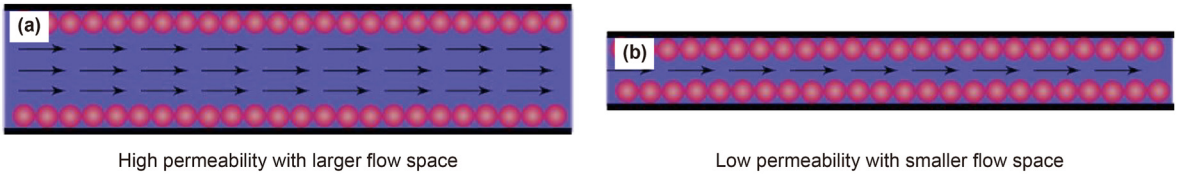

Fig. 12. Illustration of the effects of oil saturation and pore size on the pressure reduction by NPs.

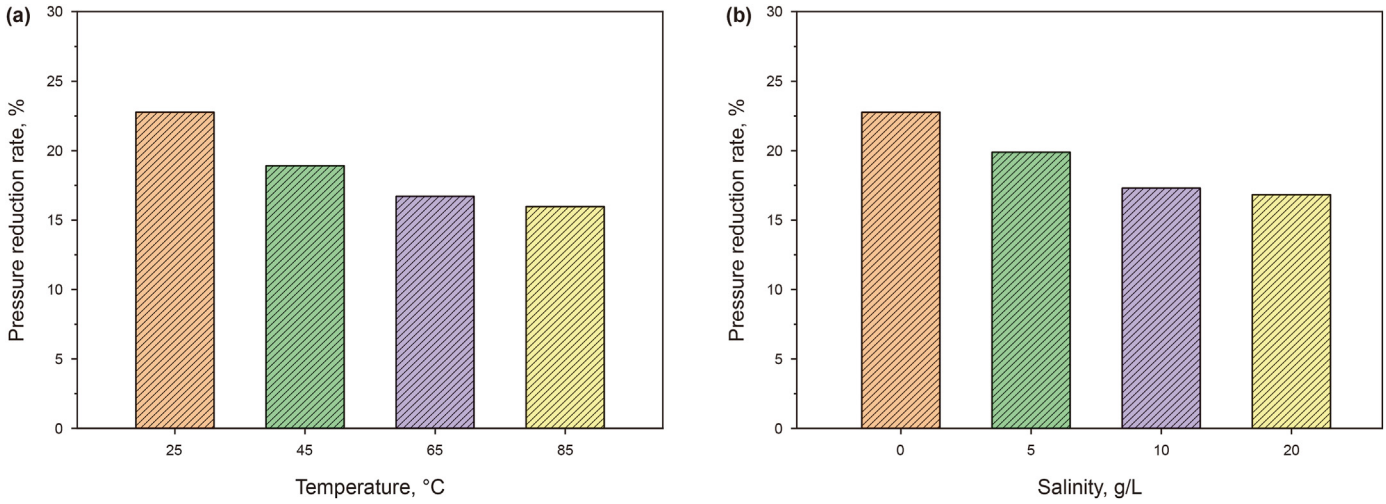

Fig. 13. Pressure reduction rate at different temperatures (**a**) and salinity levels (**b**).

the investigation of Park et al. (2013), it is recognized that the microstructural changes brought about by nanoparticle adsorption generate velocity slip, with the extent of slip in laminar flow being independent of the Reynolds number. This makes us believe that the observed transformation in flow field shape can be attributed to the phenomenon of boundary layer velocity slip, and the degree of

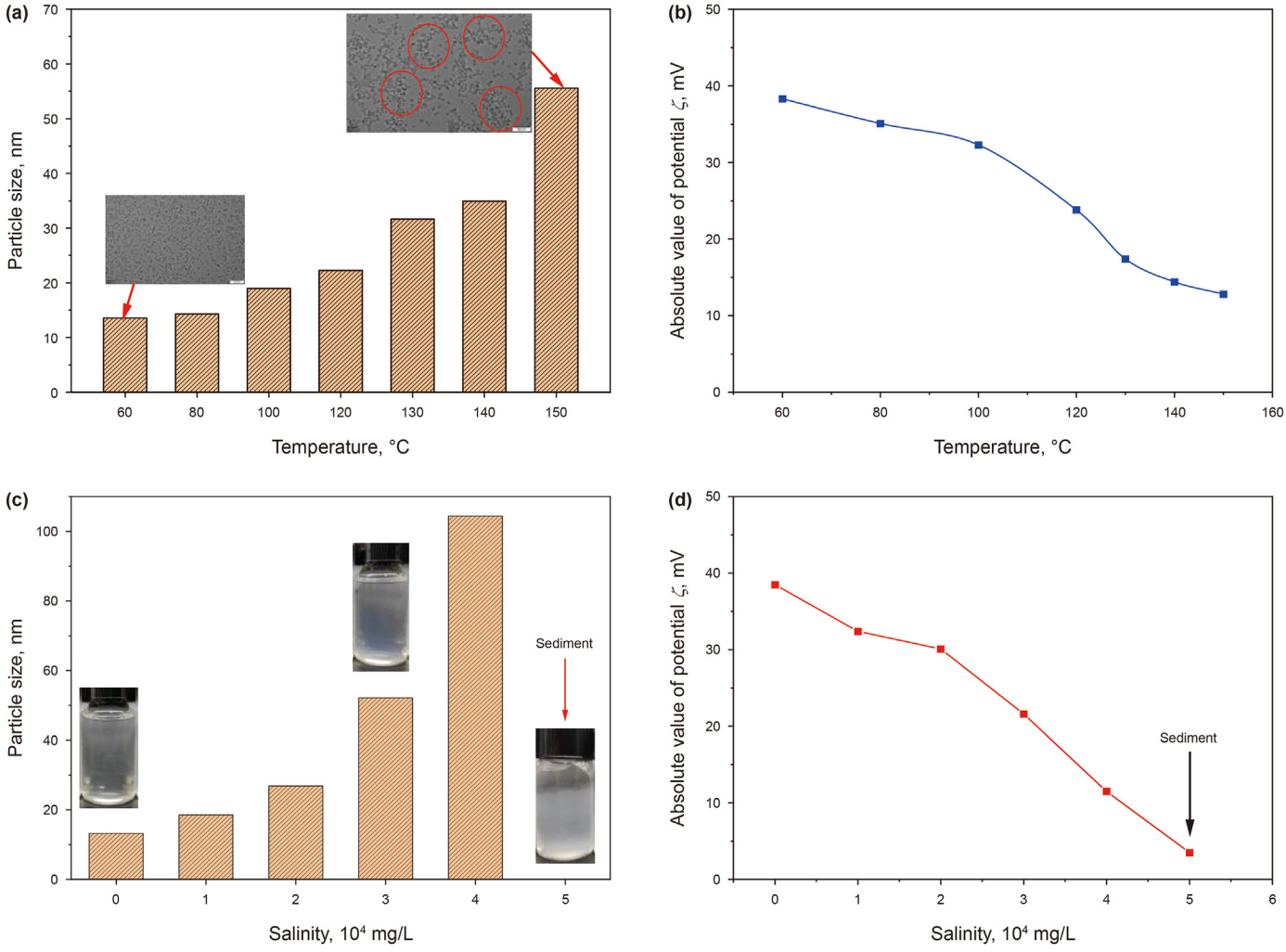

Fig. 14. Effects of temperature (**a**, **b**) and salinity (**c**, **d**) on the stability of NP dispersion solution.

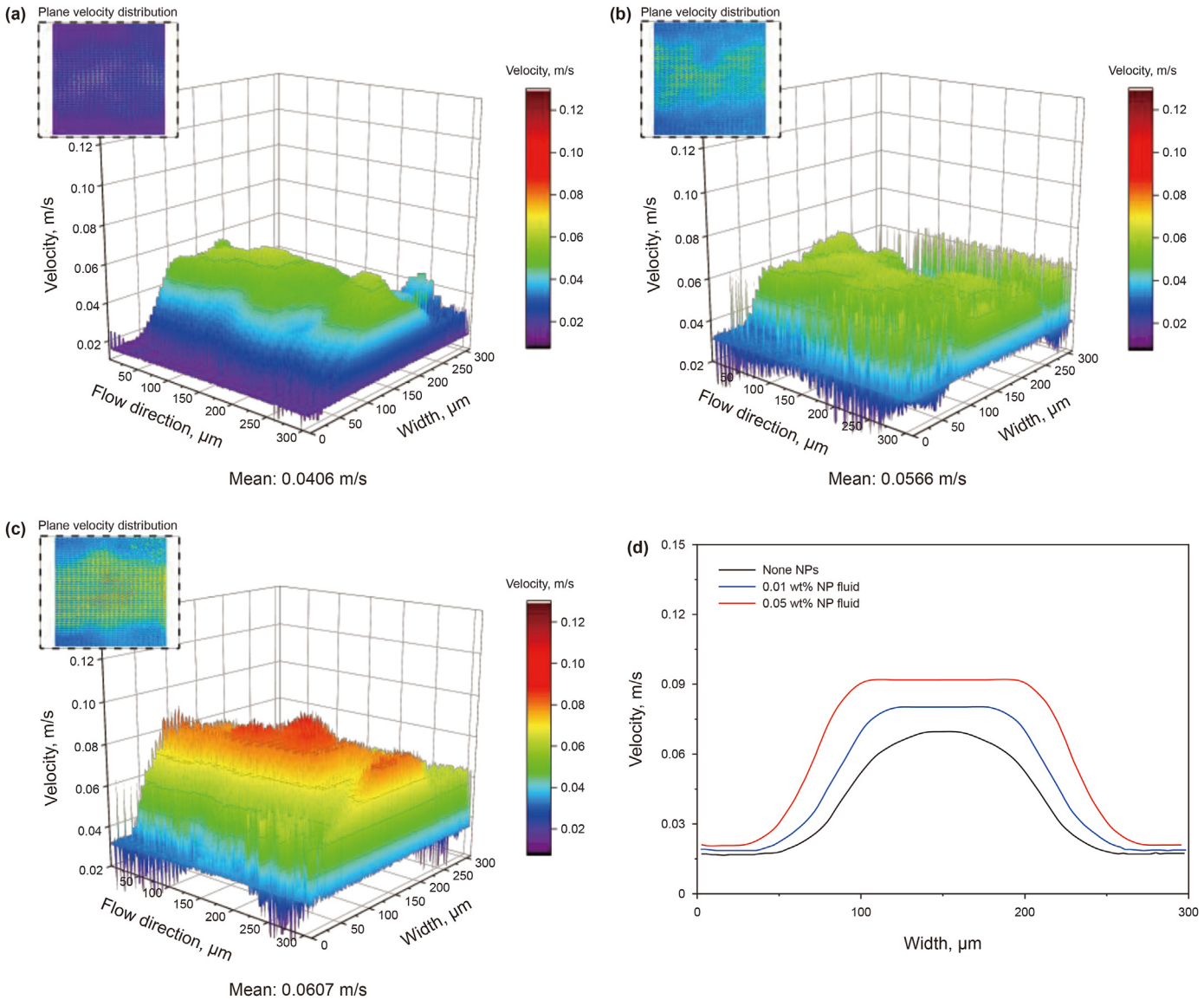

Fig. 15. Variation of local flow field in the microchannel at a pressure difference of 1.5 kPa and NP concentration of 0 (**a**), 0.01 wt% (**b**), and 0.05 wt% (**c**). (**d**) Variation of flow field cross-section shape.

slippage remains consistent at injection pressures of 1.5 and 2.5 kPa.

When the injection pressure is 1.5 kPa, the flow field is less influenced by the central throat, therefore, the flow field becomes more “flatten” after NP adsorption (Fig. 17(a) and (b)). Conversely, at an injection pressure of 2.5 kPa, a higher velocity leads to a notable influence of the central throat on flow field, so the flow filed becomes “sharper” after NP treatment (Fig. 17(c) and (d)).

The outcomes of PIV experiments show a direct indication that the adsorption of NPs onto the wall of flow channel results in a reduction of flow resistance. The mechanisms underlying the reduction in flow resistance can be elucidated through the examination of wettability experiments. Fig. 18 illustrates the experimental findings derived from wettability measurements conducted on core slices and microfluidic systems before and subsequent to the adsorption of NPs.

Based on the wettability experimental findings, it is evident that NP adsorption enhances hydrophilicity on both core slices and microfluidic chips. While a lot of studies have highlighted the hydrophobic surface potential to alleviate water flow resistance by generating a sliding interface (Cai et al., 2016; Gao et al., 2020), our experiments reveal an alternate mechanism wherein the adsorption of hydrophilic NPs on the interface similarly leads to reduced flow resistance. This observation can be explained by Ma's investigation (Ma et al., 2021), which proposes the formation of a dynamic solvation layer encompassing hydrophilic nanoparticles. When these nanoparticles absorb on the rock surface and water flow upon the surface, the NPs' solvation layer interfaces directly contact with the fluid. This dynamic solvation layer has a smaller velocity discrepancy with the internal fluid relative to the static water film created through direct wall-fluid contact.

In conclusion, the mechanism by which NPs promote pressure

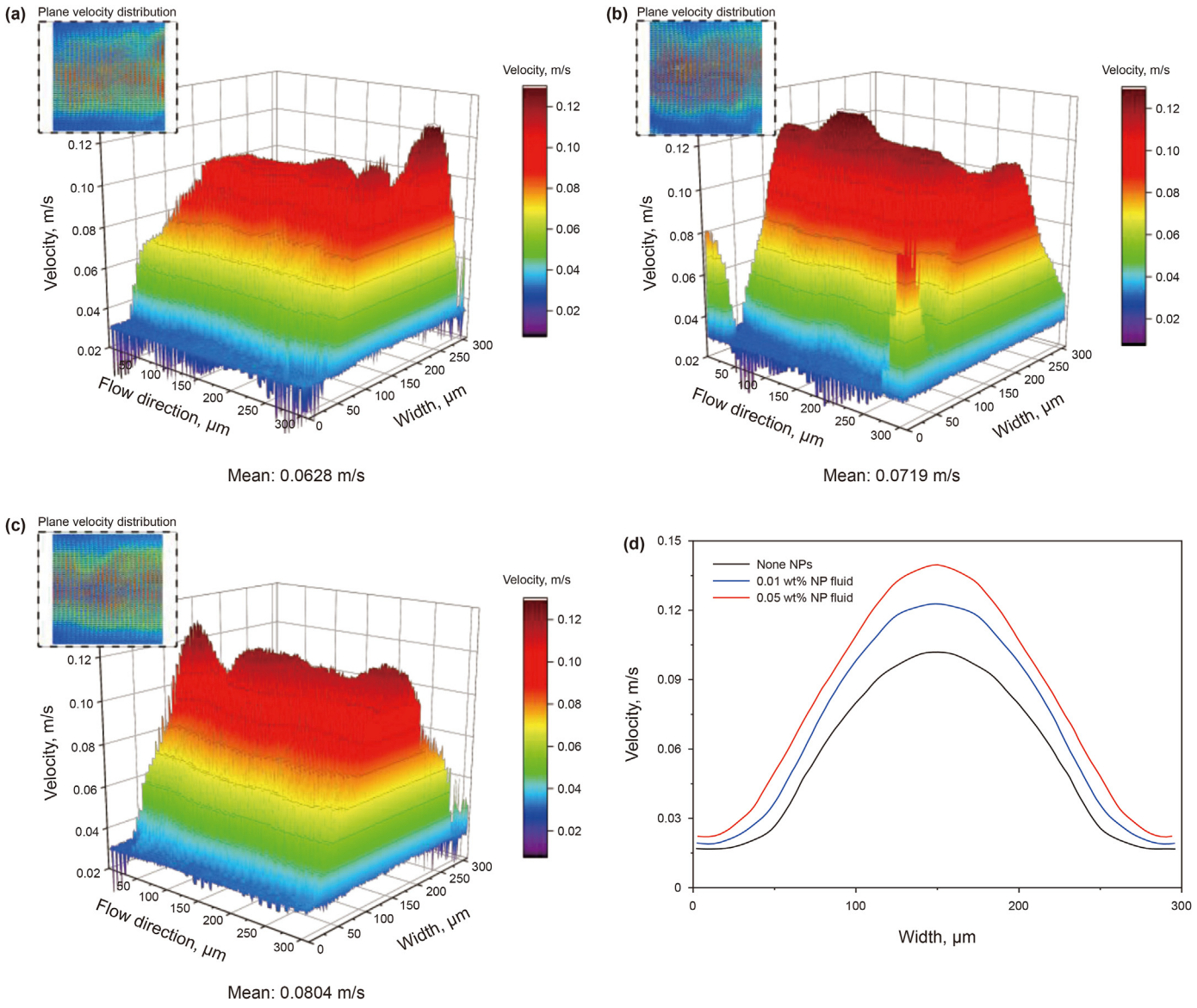

Fig. 16. Variation of local flow field in the microchannel at a pressure difference of 2.5 kPa and NP concentration of 0 (**a**), 0.01 wt% (**b**), and 0.05 wt% (**c**). (**d**) Variation of flow field cross-section shape.

reduction and augmented injection is multi-dimensional. On a microscopic scale, the presence of NPs can make wettability of fluid-solid surface more hydrophilic and increase the flow velocity. This microscopic mechanism for reducing fluid drag resistance is reflected in the macroscopic core as decreased pressure and increased fluid injection. However, for more complex macroscopic cores, factors such as particle size, stability, the environment of the reservoir, and the physical properties of the NPs have significant impacts on the effectiveness of reducing pressure and increasing fluid injection. Therefore, considering these factors comprehensively is crucial in ensuring that NPs effectively reduce pressure and increase fluid injection in practical applications.

4. Conclusions

In this study, we aimed to shed light on the pressure reduction mechanisms by NPs through the use of core displacement and microfluidic experimental systems. Our key findings are

(1) Ultra-low permeability cores treated with NPs showed a significant pressure reduction rate of 22.7% at the macroscopic scale.
(2) The effect of NPs on pressure reduction was observed to follow three modes: (i) an initial increase followed by a decrease with increasing dispersion concentration, (ii) an increase with adsorption time followed by stabilization, and (iii) an increase with core permeability and oil saturation.
(3) At the mesoscopic scale, the presence of NPs improved the fluid flow within pores by wettability alteration, resulting in enhanced fluid velocity profiles and the macroscopic effects of pressure reduction and augmented injection.

In conclusion, the use of NPs holds great promise for pressure reduction and increased injection in low-permeability and ultra-

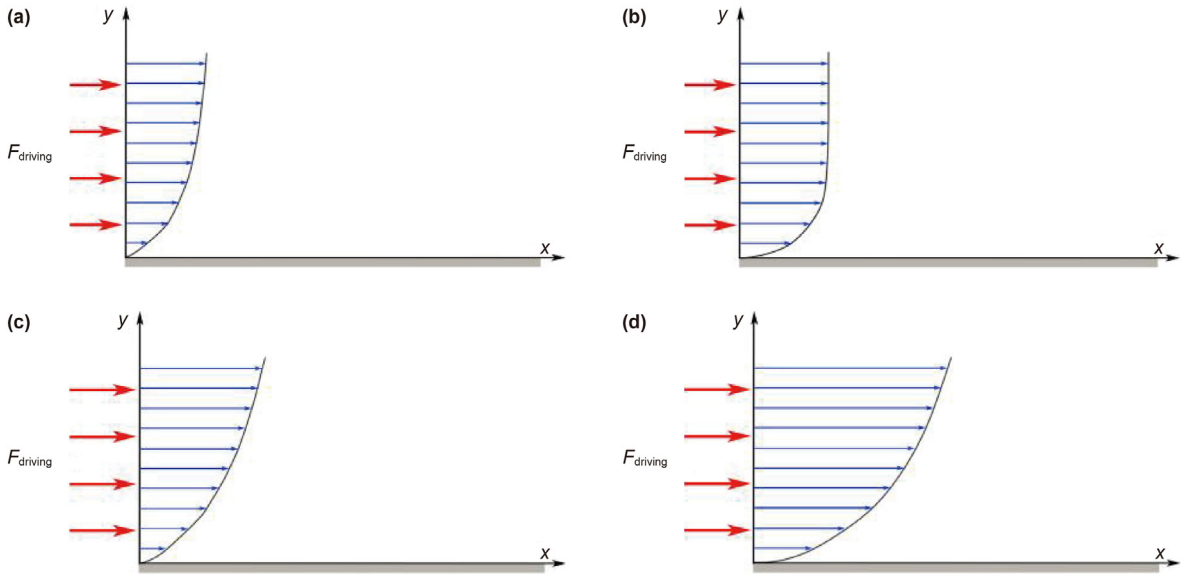

Fig. 17. Velocity distribution at different experimental conditions. (**a**) 1.5 kPa, without NPs; (**b**) 1.5 kPa, with NPs; (**c**) 2.5 kPa, without NPs; (**d**) 2.5 kPa, with NPs.

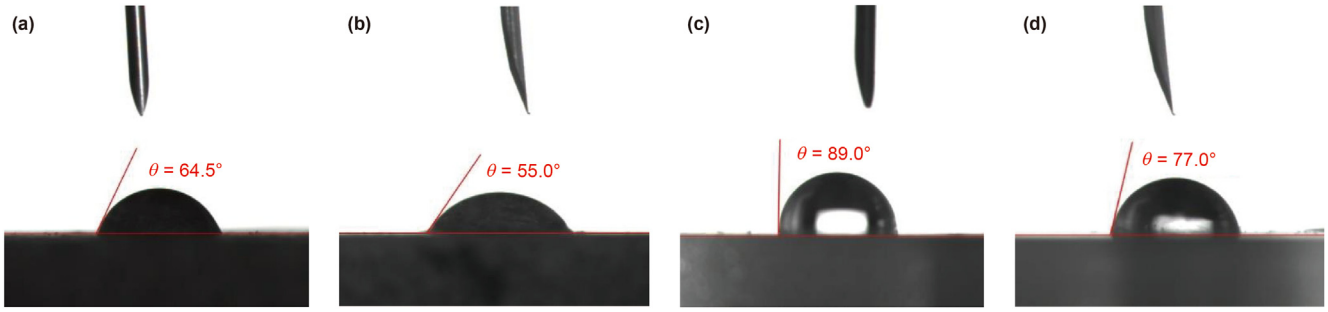

Fig. 18. Contact angle (θ) between water and solid: (**a**) Core slice before adsorption; (**b**) Core slice after adsorption; (**c**) Microfluidic chips before adsorption; (**d**) Microfluidic chips after adsorption.

low-permeability reservoirs. It is necessary to take into consideration specific reservoir conditions, and choose appropriate temperature-resistant and salinity-resistant NPs, and optimize the concentration, injection volume, and adsorption time through core experiments in order to maximize their benefits.

CRediT authorship contribution statement

Pan Wang: Conceptualization, Data curation, Formal analysis, Investigation, Methodology, Writing – original draft, Writing – review editing, Visualization. **Yu-Hang Hu:** Data curation, Investigation, Writing – original draft. **Liao-Yuan Zhang:** Resources. **Yong Meng:** Resources. **Zhen-Fu Ma:** Resources. **Tian-Ru Wang:** Validation. **Zi-Lin Zhang:** Resources. **Ji-Chao Fang:** Resources. **Xiao-Qiang Liu:** Writing – review editing. **Qing You:** Conceptualization, Funding acquisition, Investigation, Methodology, Project administration, Resources, Supervision, Writing – review editing. **Yan Zhang:** Investigation, Project administration, Supervision.

Acknowledgments

This work was supported by the National Natural Science Foundation of China (Nos. 52074249, U1663206, 52204069), and Fundamental Research Funds for the Central Universities.

References

Ali, J.A., Kolo, K., Manshad, A.K., et al., 2018. Recent advances in application of nanotechnology in chemical enhanced oil recovery: effects of nanoparticles on wettability alteration, interfacial tension reduction, and flooding. Egypt. J. Petrol. 27 (4), 1371–1383. https://doi.org/10.1016/j.ejpe.2018.09.006.

Asif, M., Muneer, T., 2007. Energy supply, its demand and security issues for developed and emerging economies. Renew. Sustain. Energy Rev. 11 (7), 1388–1413. https://doi.org/10.1016/j.rser.2005.12.004.

Cai, C., Sang, N., Teng, S., et al., 2016. Superhydrophobic surface fabricated by spraying hydrophobic R974 nanoparticles and the drag reduction in water. Surf. Coating. Technol. 307, 366–373. https://doi.org/10.1016/j.surfcoat.2016.09.009.

Cottin, B.C., Barrat, J.L., Bocquet, L., et al., 2003. Low-friction flows of liquid at nanopatterned interfaces. Nat. Mater. 2 (4), 237–240. https://doi.org/10.1038/nmat857.

Dai, C.L., Wang, S.L., Li, Y.Y., et al., 2015. The first study of surface modified silica nanoparticles in pressure-decreasing application. RSC Adv. 5 (76), 61838–61845. https://doi.org/10.1039/c5ra09883a.

Ding, B.J., 2004. Progress in nano-science, engineering and technology. Nanosci. Technol. 2, 9–10 (in Chinese).

Di, Q.F., Gu, C.Y., Shi, L.Y., et al., 2007. Pressure drop mechanism of enhancing water injection technology with hydrophobicity nanometer SiO_2. Drill. Prod. Technol. 30 (4), 1–94. https://doi.org/10.3969/j.issn.1006-768X.2007.04.030 (in Chinese).

Gao, D., Bai, M., Hu, C., et al., 2020. Hydrophobic surface-assisted SiO_2/DI-water nanofluids for enhancing heat transfer and reducing flow resistance. Nanotechnology 32 (12). https://doi.org/10.1088/1361-6528/abd0b3.

Hendraningrat, L., Torsæter, O., 2014. Effects of the initial rock wettability on silica-based nanofluid-enhanced oil recovery processes at reservoir temperatures. Energy Fuel. 28 (10), 6228–6241. https://doi.org/10.1021/ef5014049.

Hu, C.H., Zhang, Y., Yang, Z., et al., 2020. Experimental study on functional characteristics of pH-sensitive nanoparticles for pressure reduction and augmented injection in tight oil reservoir. J. Mol. Liq., 113253 https://doi.org/10.1016/

j.molliq.2020.113253.
Hu, W.R., Wei, Y., Bao, J.W., 2018. Development of the theory and technology for low permeability reservoirs in China. Petrol. Explor. Dev. 45 (4), 685–697. https://doi.org/10.11698/PED.2018.04.10 (in Chinese).
Idris, A., Man, Z., Maulud, A.S., et al., 2020. Investigation on particle properties and extent of functionalization of silica nanoparticles. Appl. Surf. Sci. 506 (15), 144978. https://doi.org/10.1016/j.apsusc.2019.144978.
Kaibo, Z., Xiang, Z., Jie, L., et al., 2020. Application of magnetic nanoparticles in petroleum industry: a review. J. Petrol. Sci. Eng. 188, 106943. https://doi.org/10.1016/j.petrol.2020.106943.
Ke, Y.C., Wei, G.Y., 2008. Application and development of nanomaterials in oil drilling and recovery. Oilfield Chem 25 (2), 189–192. https://doi.org/10.3969/j.issn.1000-4092.2008.02.024 (in Chinese).
Kong, L., Zhang, L., Bao, Y., et al., 2022. Effect of surface roughness and particle size on lubrication mechanisms of SiO_2 nanoparticles. Adv. Mater. Sci. Eng. https://doi.org/10.1155/2022/7051650.
Lauga, E., Brenner, M.P., Stone, H.A., 2007. Microfluidics: the No-Slip Boundary Condition. Springer Berlin Heidelberg, pp. 1219–1240. https://doi.org/10.48550/arXiv.cond-mat/0501557.
Lu, X.L., Lv, G.Z., Luan, Z.A., et al., 2003. Application of polesilicon in low permeability oil field. Petrol. Explor. Dev. 30 (6), 110–112. https://doi.org/10.3321/j.issn:1000-0747.2003.06.034 (in Chinese).
Ma, A.J., Chen, S.J., Li, Y.X., et al., 2021. Molecular dynamics simulation of Brownian diffusion boundary condition for nanoparticles. Acta Phys. Sin. 70 (14), 148201. https://doi.org/10.7498/aps.70.20202240 (in Chinese).
Nikolov, A., Kondiparty, K., Wasan, D., 2010. Nanoparticle self-structuring in a nanofluid film spreading on a solid surface. Langmuir 26 (11), 7665–7670. https://doi.org/10.1021/la100928t.
Park, H., Park, H., Kim, J., 2013. A numerical study of the effects of superhydrophobic surface on skin-friction drag in turbulent channel flow. Phys. Fluids 25 (11), 110815. https://doi.org/10.1063/1.4819144.
Qu, C.Y., 2008. Poly silicon nanometer augmented injection technology in the application of the low permeability reservoir. Inn. Mong. Petrochem. Ind. 10, 225–227 (in Chinese).
Roustaei, A., Saffarzadeh, S., Mohammadi, M., 2013. An evaluation of modified silica nanoparticles' efficiency in enhancing oil recovery of light and intermediate oil reservoirs. Egypt. J. Petrol. 22 (3), 427–433. https://doi.org/10.1016/j.ejpe.2013.06.010.
Suleimanov, B.A., Ismailov, F.S., Veliyev, E.F., 2011. Nanofluid for enhanced oil recovery. J. Petrol. Sci. Eng. 78 (2), 431–437. https://doi.org/10.1016/j.petrol.2011.06.014.
Sun, Z.G., Wei, L.X., Guo, H., et al., 2006. Experimental study on injection augmentation of polysilicon nanomaterials in low permeability fields of Chunliang. J. Oil Gas Technol. (J. Jianghan Petroleum Inst.) 28 (1), 105–107. https://doi.org/10.3969/j.issn.1000-9752.2006.01.034 (in Chinese).
Turan, N.B., Erkan, H.S., Engin, G.O., et al., 2019. Nanoparticles in the aquatic environment: usage, properties, transformation and toxicity—a review. Process Saf. Environ. Protect. 130, 238–249. https://doi.org/10.1016/j.psep.2019.08.014.
Wang, K.L., Liang, S.C., Wang, C.C., 2003. Research of improving water injection effect by using active SiO_2 nano-powder in low-permeability oilfield. China Powder Sci. Technol. 15, 179–182. www.scientific.net/AMR.92.207.
Wang, L., Li, Z., Mao, G., et al., 2022. Effect of nanoparticle adsorption on the pore structure of a coalbed methane reservoir: a laboratory experimental study. ACS Omega 7 (7), 6261–6270. https://doi.org/10.1021/acsomega.1c06770.
Wang, T.R., Zhang, Y., Li, L., et al., 2018. Experimental study on pressure-reduction performance and mechanism of nanoparticles in low permeability reservoir. J. Petrol. Sci. Eng. 166, 693–703. https://doi.org/10.1016/j.petrol.2018.03.070.
Wasan, D.T., Nikolov, A.D., 2003. Spreading of nanofluids on solids. Nature 423 (6936), 156–159. https://doi.org/10.1038/nature01591.
Yekeen, N., Padmanabhan, E., Idris, A.K., et al., 2019. Nanoparticles applications for hydraulic fracturing of unconventional reservoirs: a comprehensive review of recent advances and prospects. J. Petrol. Sci. Eng. 178, 41–73. https://doi.org/10.1016/j.petrol.2019.02.067.
Zhai, H.L., Qi, N., Fan, J.C., et al., 2018. Research progress of relative permeability modifiers system used in oilfield. Oilfield Chem. 35 (2), 375–380. https://doi.org/10.19346/j.cnki.1000-4092.2018.02.034 (in Chinese).
Zhang, H., Nikolov, A., Wasan, D., 2014. Enhanced oil recovery (EOR) using nanoparticle dispersions: underlying mechanism and imbibition experiments. Energy Fuel. 28 (5), 3002–3009. https://doi.org/10.1021/ef500272r.
Zheng, Z.H., Li, D.H., Wang, Z.X., et al., 2017. Assessment of potential of tight oil and gas in major basins in China. China Min. Mag. 26 (8), 22–29 (in Chinese).